

Refining Higher-order Bulk-boundary Correspondence of Corner-localized States

Minwoo Jung,^{1,*} Yang Yu,² and Gennady Shvets^{2,†}

¹*Department of Physics, Cornell University, Ithaca, New York, 14853, USA*

²*School of Applied and Engineering Physics, Cornell University, Ithaca, New York 14853, USA*

(Dated: October 21, 2020)

We demonstrate that a corner-localized state may fail to be a relevant indicator of a non-trivial higher-order topological invariant, even though their existence conditions appear to coincide with each other. Our analysis of C^n -symmetric crystalline insulators and their multilayer constructions reveals that corner states are not necessarily correlated with other well-established higher-order topological observables such as fractional corner charge or filling anomaly. We refine several bulk-corner correspondences that have been imprecisely conjectured based on the emergence of corner-localized states. An important example is that the zero-energy corner states in a breathing Kagome lattice are induced by decoration of topological edges and cannot be explained as a direct result of the bulk polarization. Our work urges more solid theoretical grounds in future works when corner states are claimed to be associated with higher-order topology of host materials.

Bulk-boundary correspondence (BBC) lies at the heart of topological physics, as it bridges abstract mathematical indices called topological invariants, which are calculated from band structures of a bulk material, to physical observables at its boundary. Early efforts in establishing BBC focused on boundaries of co-dimension 1 such as edges of two-dimensional (2D) materials or surfaces of three-dimensional (3D) materials [1–5]. Inspired by the discovery—both theoretical[6–10] and experimental[11–15]—of topological materials that feature gapless states at boundaries of co-dimension $d \geq 2$, efforts have recently been made to extend the framework of BBC to these higher-order topological phases [16–18]. The study of BBC sometimes takes a form of analytic case studies with a specific form of topological invariant [3, 4, 18], or relies on algebraic topology for generic classification of bulk and boundary Hamiltonians [1, 2, 5, 16, 17]. While the latter approach provides more comprehensive formulation of BBC than the former does, its concern does not aim further than identifying the classification group of Hamiltonian in certain symmetry classes, thereby evading the task of finding the actual topological invariants relevant to the boundary signatures.

In this sense, the algebraic classification method allows an insightful start for the search of topological structures, but solid BBC cannot be established without complementary roles of rigorous case studies. As the field of higher-order topological insulators (HOTIs) hastily grew popular, however, a rigorous BBC has been often neglected that some boundary signatures—especially, corner-localized states—were entitled to be topological without clear causal relations to suggested bulk invariants. To be specific, the following framework has been widely exploited in the field of HOTI in recent years: (1) find a symmetry-protected bulk topological invariant of a given Hamiltonian model, (2) show that a corner-localized state appears when the Hamiltonian parameter condition gives rise to nontrivial bulk invariant, and (3) conclude that the corner state is topological because

the phase diagram of its existence condition is identical to that of the bulk invariant. To rightly claim that a boundary signature stems from a topological origin, however, there needs to be a physical explanation how the bulk invariant leads to the emergence of the anomalous boundary properties. Otherwise, a topological nature of a boundary can be attributed to an irrelevant bulk invariant, or a trivial defect state can be mistaken to be considered topological, thereby obscuring true BBC.

In this Letter, we address several cases of such misrepresented higher-order BBC, specifically in the context of corner-localized states and bulk polarization in 2D C^n -symmetric topological crystalline insulators (TCIs). The multilayer stacking construction of TCIs [19] reveals that the zero-energy corner states (ZCSs) in C^3 -symmetric TCI (also known as breathing Kagome lattices) [19–23] are purely an edge effect associated with \mathbb{Z}_2 composite Zak-phase of chiral edge bands and are not well correlated with the bulk polarization characterized by \mathbb{Z}_3 . Also, we discuss that the ZCSs in 4-band C^4 -symmetric TCI model [15, 19, 20, 24] should not be attributed to the bulk polarization of the lowest energy band only, as the chiral symmetry plays an essential role in their existence. These examples clearly demonstrate that a precise formulation of BBC requires more than simply identifying the phase diagrams of a bulk invariant and a boundary signature.

Before we begin to refine those ill-defined BBCs, let us list out some well-established BBCs for comparison. A classic example is hall conductivity and Chern number, as they are directly related through an analytic expression [25]. Since conduction cannot occur in an insulating bulk, nonzero hall conductivity in a Chern insulator must indicate metallic channels on its edge or, in other words, gapless edge states [26]. Another analytically straightforward BBC is found between fractional edge charge and bulk polarization in a one-dimensional (1D) TCI [27], i.e. Su-Schrieffer-Heeger (SSH) model, and recent works [19, 28] have established higher-order version of similar

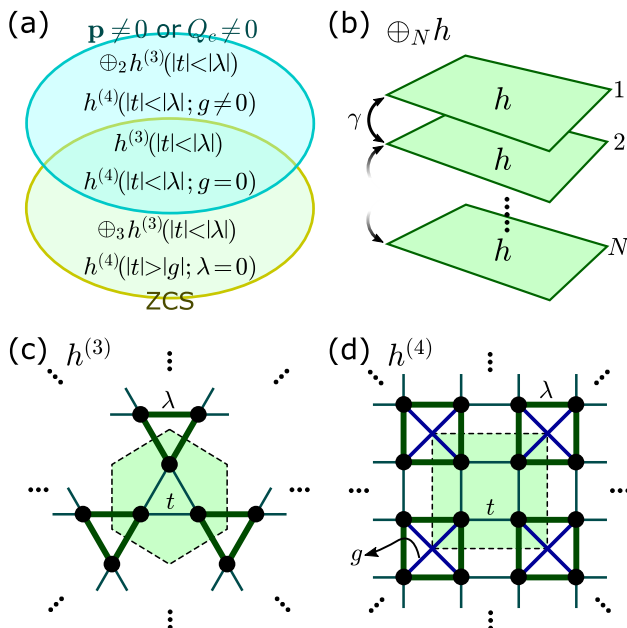


FIG. 1. (a) A Venn diagram classification of C^3 - and C^4 -symmetric crystalline insulators in regard to the existence of nonzero \mathbf{p}/Q_c and the existence of ZCSs. (b) N -layer stacking of a Hamiltonian model h , $\oplus_N h$; γ denotes the interlayer coupling strength. (c) C^3 -symmetric crystalline insulator model $h^{(3)}$; t and λ are the nearest-neighbor coupling within and across unit cells, respectively. (d) C^4 -symmetric crystalline insulator model $h^{(4)}$; g is the next-nearest-neighbor coupling across diagonally adjacent unit cells.

correspondences in 2D TCIs by constructing bulk invariants explicitly for fractional corner charges. Even though these boundary anomalies in the form of fractional charge excess/deficit have yet to be incorporated in the framework of the algebraic classification method [17], they are lately gaining attention as an alternative probe of higher-order topology [20].

A key result of this work is that fractional corner/edge charge anomalies are neither a sufficient nor necessary condition for the existence of ZCSs unlike nonzero hall conductivity being a necessary and sufficient condition for gapless edge states. Figure 1(a) provides a Venn diagram summarizing our case studies of C^n -symmetric TCI models in terms of their bulk polarization \mathbf{p} , secondary topological index for corner charge Q_c (following the definition given in Ref. [19]), and the existence of ZCSs. It clearly illustrates that a ZCS can arise despite vanishing \mathbf{p} and Q_c or that a ZCS might not exist despite non-trivial \mathbf{p} and Q_c . The stacking operation \oplus between two crystalline insulators h_1 and h_2 is defined as [19]

$$h_1 \oplus h_2 = \begin{bmatrix} h_1 & \gamma \\ \gamma^\dagger & h_2 \end{bmatrix}, \quad (1)$$

where γ describes the nearest-neighbor coupling between adjacent layers. The strength of interlayer coupling is

set to be reasonably small so that the shared bandgap of $h_{1,2}$ is not closed. We denote an N layer stack of h as $\oplus_N h$, as depicted in Fig. 1(b). This operation allows us to easily access other topologically distinct phases, as the topological indices of a stacked insulator are simply given as addition of those in each layer [19]; for example,

$$\mathbf{p}_{h_1 \oplus h_2} \equiv \mathbf{p}_{h_1} + \mathbf{p}_{h_2} \pmod{\{\mathbf{R}\}}, \quad (2)$$

where the composite polarization \mathbf{p} (normalized to a unit charge) is evaluated in each model for all bands below the shared bandgap of interest, and is given in modulo the set of primitive lattice vectors $\{\mathbf{R}\}$. The same relation holds for Q_c as well in modulo unit charge. Figure 1(c)-(d) illustrate C^3 - and C^4 -symmetric crystalline insulator models, respectively, along with their tight-binding parameters.

When the nearest-neighbor coupling strengths across unit cells, λ , are greater than those within unit cells, t , C^3 -symmetric model $h^{(3)}$ (Fig. 1(c)) carries a ZCS emerging at every 60° -angled corners of a type with a single corner-most sublattice, as depicted in Fig. 2(a) (another type of 60° -angled corners with two corner-most sublattices doesn't support ZCSs). The same condition $|t| < |\lambda|$ produces nonzero bulk polarization $\mathbf{p} = \frac{2}{3}\mathbf{R}_1 + \frac{2}{3}\mathbf{R}_2$ in the lowest energy band, which is separated from the second and third bands by a bandgap, see Fig. 2(b). Figure 2(c) illustrates the location of Wannier centers due to $\mathbf{p} = \frac{2}{3}\mathbf{R}_1 + \frac{2}{3}\mathbf{R}_2$ and the resulting charge distribution (in modulo unit charge) in the limit of $|t| \ll |\lambda|$ when the lowest energy band is filled. It is well established that nonzero bulk polarization in $h^{(3)}$ gives rise to a different type of second-order topological observables called fractional corner anomaly (FCA) $\phi = \frac{1}{3}$ [20].

Our analysis of multilayer stacking constructions of $\oplus_{1,2,3,\dots} h^{(3)} (|t| < |\lambda|)$, however, reveals that the existence of ZCSs is not correlated with nonzero bulk polarization nor with FCA, even though such correspondence has been widely assumed as the existence conditions $|t| < |\lambda|$ for ZCSs and nonzero \mathbf{p} appear to coincide with each other. It turns out that the (composite) Zak phase of edge bands is instead responsible for the emergence of ZCSs. Figure 2(d) shows the band dispersion of 1D-periodic nano-ribbon structure terminated by an edge shown in Fig 2(a), where the red line denotes an edge-localized band. The edge band carries the inversion eigenvalues of $+1$ at $k_{edge} = 0$ and -1 at $k_{edge} = 0.5$, thereby featuring a Zak phase of π [27] (or polarization of $\frac{1}{2}$ [28]). The energy dispersion of this band follows $E_{edge} = -\sqrt{t^2 + \lambda^2 + 2t\lambda \cos(2\pi k_{edge})}$, which is reminiscent of a 1D chiral-symmetric SSH chain [27]. In fact, the chiral partner band of this edge band in Fig. 2(d) does not stand out since it is hybridized with other bulk bands at positive energy. In this sense, the corner-most sublattice in Fig. 2(a) can be interpreted as a dislocation in an edge-localized chiral-symmetric SSH chain, and it

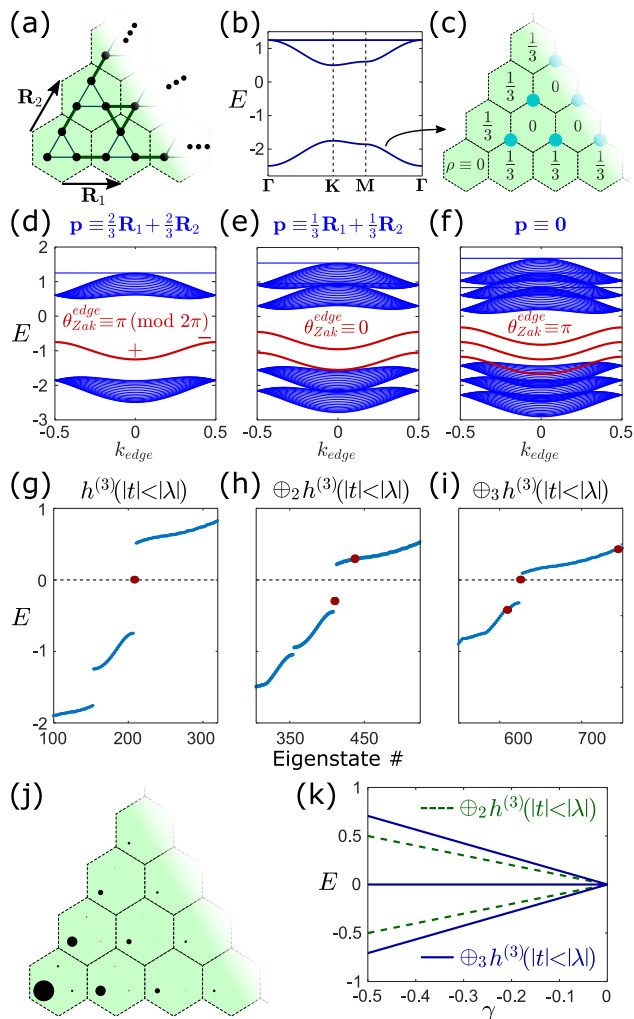


FIG. 2. (a) A 60° -angled corner with a single corner-most sublattice. (b) Band structure of $h^{(3)}$; $t = -0.25$ and $\lambda = -1$. (c) Charge distribution around a 60° -angled corner at $\frac{1}{3}$ -filling (upto the first band only); turquoise circles denote the positions of the wannier centers. (d) Edge dispersion of nanoribbon structure with an edge termination like one of the edges in (a); the edge localized band is colored red along with its inversion eigenvalues at high symmetry points. (e)-(f) Edge dispersion of bilayer and trilayer stacked structures, respectively. (g)-(i) Eigenspectra of mono-, bi-, and trilayer structures, respectively, with open boundaries (190 unit cells) of triangular termination like in (a); corner-localized modes are highlighted as dark red dots, and $\gamma = -0.3$. (j) Field profile of a ZCS in (g) or (i); the radii of black circles are proportional to the wavefunction amplitude. (k) Energies of corner-localized states in bilayer(dotted green) and trilayer(solid blue) structures as a function of γ .

is well known that such dislocation hosts a ZCS as a consequence of Zak phase of π [27]. We indeed observe the well-known ZCS of $h^{(3)}$ ($|t| < |\lambda|$) as shown in Fig. 2(g) and (j).

Bilayer and trilayer stacks of $h^{(3)}$ ($|t| < |\lambda|$), according to Eq. (2), carry the bulk polarization of $\mathbf{p} = \frac{1}{3}\mathbf{R}_1 + \frac{1}{3}\mathbf{R}_2$

and $\mathbf{p} = \mathbf{0}$, respectively. Thus, if we classify these structures based on their bulk polarization, $\oplus_2 h^{(3)}$ is in a topologically nontrivial phase and $\oplus_3 h^{(3)}$ is trivial. This distinction will indeed physically manifest in their FCA; $\phi = \frac{2}{3}$ for $\oplus_2 h^{(3)}$, and $\phi = 0$ for $\oplus_3 h^{(3)}$. On the other hand, if we examine the composite Zak phase of the edge-localized bands in those structures, as shown in Fig. 2(e)-(f), the bilayer stack features vanishing edge Zak phase (modulo 2π) and the trilayer stack has nontrivial π edge Zak phase. In the presence of multiple bands below a certain bandgap of interest, the existence of a mid-gap boundary/dislocation state in 1D systems is determined by the composite Zak phase of all bands below the bandgap [29, 30]. As expected, we find that $\oplus_2 h^{(3)}$ lacks any ZCS, whereas $\oplus_3 h^{(3)}$ possesses a ZCS, see Fig. 2(h)-(i).

We note that there exist two corner-localized states in the bilayer stack structure as well, but they are not pinned at zero-energy. Their spectral positions are at $E = \pm\gamma$, where γ is the interlayer coupling strength, see Fig. 1(b). Consequently, these corner states are not spectrally stable against some perturbations in γ . Similarly, the trilayer stack also carries two spectrally unstable corner states at $E = \pm\sqrt{2}\gamma$ other than the ZCS. The spectral shifts of these corner states with respect to the change in γ is drawn in Fig. 2(k). In general, $\oplus_N h^{(3)}$ ($|t| < |\lambda|$) carries N corner-localized states, and only one of them becomes a ZCS when N is an odd number. For example, both the monolayer and the four-layer stack structures possess nontrivial bulk polarization $\mathbf{p} = \frac{2}{3}\mathbf{R}_1 + \frac{2}{3}\mathbf{R}_2$, but only the former carries a ZCS per corner. Also, both the trilayer and the six-layer stack structures are trivial in their bulk polarization of $\mathbf{p} = \mathbf{0}$, but the former still carries a ZCS per corner. Therefore, it is clear that the existence of ZCSs is determined not by \mathbb{Z}_3 bulk polarization, but by \mathbb{Z}_2 edge band Zak phase.

Next, we show that the ZCS in C^4 -symmetric TCI, $h^{(4)}$ ($|t| < |\lambda|$; $g = 0$) from Fig. 1(d), is a result of a half corner charge from the lower two bands in the presence of chiral symmetry, not a result of the bulk polarization from the lowest band. The chiral symmetry in C^4 -symmetric TCI is given as $S = \text{diag}[1, -1, 1, -1]$ where the four sublattices are indexed in a clockwise order, and its presence $Sh^{(4)}S^{-1} = -h^{(4)}$ gives rise to a band structure that is mirror-symmetric with respect to the zero energy. It is well studied in various systems [7, 8, 12–15, 19, 28, 31] that the combination of a half fractional corner charge and the chiral symmetry guarantees a ZCS. If the bands below zero energy carry a half charge at a corner, the chiral symmetry ensures that the bands above zero energy also carry a half charge at the corner. Since the integration of local density of states over energy must be equal to the number of bands at each unit cell, the fractional corner charge in this case cannot be a charge surplus as it implies that the integration at the corner unit cell exceeds the number of bands. Thus, two half

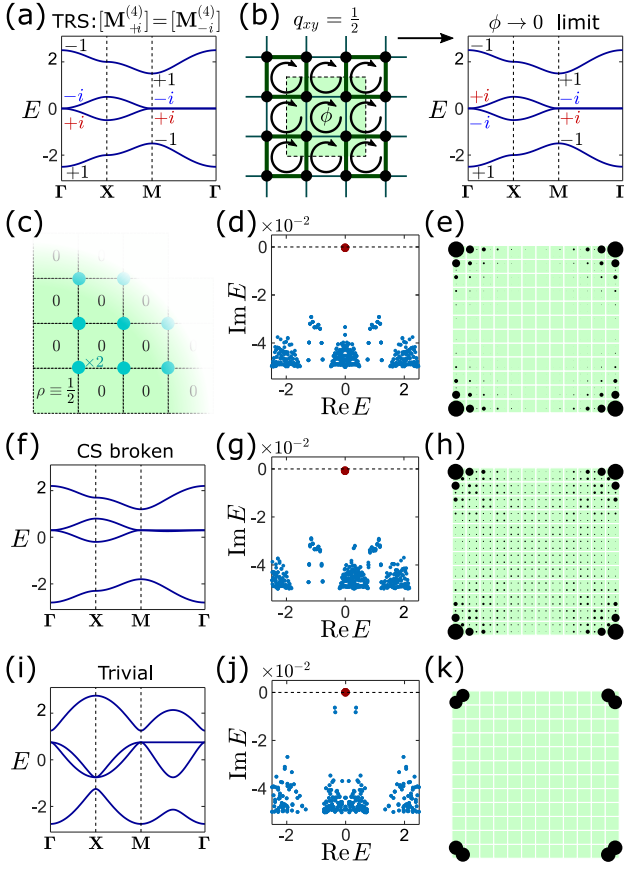


FIG. 3. (a) Band structure of $h^{(4)}$ along with C^4 -rotation eigenvalues at Γ and M ; $t = -0.25$, $\lambda = -1$, and $g = 0$. (b) The same structure in (a) viewed as a zero-flux limit ($\phi \rightarrow 0$) of quadrupole insulator. (c) Charge distribution around a corner at half-filling (upto the second band); two wannier centers (turquoise circles) are overlapping at each position. (d) Eigenvalues in a complex energy plane; a uniform on-site loss of $\delta = 0.05$ was applied to an open-boundary domain of 12×12 unit cells except at each 2×2 corner unit cells. (e) Field profile of the modes marked as dark red dots in (d). (f)-(h) The same as (a), (d), and (e) for $t = -0.25$, $\lambda = -1$, and $g = -0.3$. (i)-(k) For $t = -1$, $\lambda = 0$, and $g = -0.75$.

charge deficits, each from the lower and the upper bands, requires the existence of a corner state to compensate for total whole charge deficit, and this corner state should be pinned at zero energy due to the chiral symmetry.

In a time reversal- and C^4 -symmetric crystalline insulator, the following expressions can be used to determine its topological indices [19]:

$$\mathbf{p} = \frac{1}{2} \left[\mathbf{X}_{+1}^{(2)} \right] (\hat{\mathbf{x}} + \hat{\mathbf{y}}) \pmod{\{\hat{\mathbf{x}}, \hat{\mathbf{y}}\}}, \quad (3a)$$

$$Q_c = \frac{1}{4} \left(\left[\mathbf{X}_{+1}^{(2)} \right] + 2 \left[\mathbf{M}_{+1}^{(4)} \right] + 3 \left[\mathbf{M}_{+i}^{(4)} \right] \right) \pmod{1}, \quad (3b)$$

where $[\mathbf{k}_p^{(n)}] \equiv \#\mathbf{k}_p^{(n)} - \#\Gamma_p^{(n)}$, and $\#\mathbf{k}_p^{(n)}$ refers to the number of eigenstates with C^n -rotation eigenvalue p at a C^n -rotational invariant momentum \mathbf{k} upto a certain number of the first few bands. For example, in

$h^{(4)}$ ($|t| < |\lambda|$; $g = 0$), the C^2 -rotation eigenvalues at \mathbf{X} and at Γ are $(-1, +1, +1, -1)$ and $(+1, -1, -1, +1)$, respectively, in order from the lowest band to the fourth band. Then, we get $[\mathbf{X}_{+1}^{(2)}] = \#\mathbf{X}_{+1}^{(2)} - \#\Gamma_{+1}^{(2)} = 0 - 1 = -1$ for the lowest band only and $[\mathbf{X}_{+1}^{(2)}] = 1 - 1 = 0$ for the first two bands together. Thus, according to Eq. (3a), the lowest band carries a nonzero bulk polarization of $\mathbf{p} = \frac{1}{2}(\hat{\mathbf{x}} + \hat{\mathbf{y}})$, but the first two bands together feature vanishing polarization $\mathbf{p} = \mathbf{0}$.

Figure 3(a) depicts the band structure of $h^{(4)}$ ($|t| < |\lambda|$; $g = 0$) model along with C^4 -rotation eigenvalues at M and at Γ . Since two degenerate modes at zero energy have different eigenvalues $\pm i$ both at M and at Γ , there arises an ambiguity of whether we assign $+i$ or $-i$ to the C^4 -rotation eigenvalue of the second band. This ambiguity, however, can be lifted up partially by the time-reversal symmetry, which enforces $[\mathbf{M}_{+i}^{(4)}] = [\mathbf{M}_{-i}^{(4)}]$, that we should choose the same values at M and at Γ . Without loss of generality, $-i$ is assigned to the second band, see Fig. 3(a), which gives $[\mathbf{M}_{+i}^{(4)}] = 1 - 1 = 0$ for the first two bands. Then, along with $[\mathbf{X}_{+1}^{(2)}] = 0$ and $[\mathbf{M}_{+1}^{(4)}] = -1$, Equation 3b yields a half corner charge $Q_c = \frac{1}{2}$ for the first two bands.

Another way of interpreting this half charge is to consider this C^4 -symmetric TCI model as a quadrupole insulator in a zero flux limit, as shown in Fig. 2(b). Any finite phase flux upon a cyclic hopping opens a complete bandgap between the second and the third band, while maintaining the chiral symmetry [15]. In this setting, the C^4 -rotation eigenvalues of the second band are different at M , $+i$, and at Γ , $-i$. While we cannot apply Eq. (3) no longer as the time-reversal symmetry is broken due to the finite flux, the quadrupole moment q_{xy} can be evaluated as

$$e^{i2\pi q_{xy}} = r_4^+(\mathbf{M})r_4^+(\mathbf{\Gamma})^* = r_4^-(\mathbf{M})r_4^-(\mathbf{\Gamma})^*, \quad (4)$$

where $r_4^\pm(\mathbf{k})$ is the C^4 -rotation eigenvalue at $\mathbf{k} = \mathbf{M}/\mathbf{\Gamma}$ that satisfies $r_4^\pm(\mathbf{k})^2 = \pm 1$ [28, 32]. From Fig. 2(b), we get $r_4^+(\mathbf{M}) = -1$, $r_4^+(\mathbf{\Gamma}) = +1$, $r_4^-(\mathbf{M}) = +i$, $r_4^-(\mathbf{\Gamma}) = -i$, and therefore $q_{xy} = \frac{1}{2}$.

As a result, the charge distribution at half-filling (upto the second band) drawn in Fig. 3(c) shows a half corner charge and vanishing edge charge, as two overlapping wannier centers from the first and second bands cancel the contribution from each other to bulk polarization. Figure 3(d)-(e) show that the expected ZCS clearly arises even though it is embedded in the bulk continuum. Following the method used in Ref. [24], we introduced a uniform loss of $-i\delta$ in the system except at small subsystems (2×2 unit cell) at each corner in order to select out the corner states, as their imaginary part of eigenvalue becomes relatively much less than other bulk modes. As soon as the chiral symmetry is broken by a finite g , see Fig. 3(f)-(g), these states get hybridized with the bulk continuum, thereby losing the corner localization, see

Fig. 3(h). This observation verifies that the presence of chiral symmetry with respect to zero energy plays a pivotal role in the existence of a ZCS, and therefore that the relevant topological indices for the ZCS should be investigated at half-filling instead at quarter-filling.

Furthermore, we report a case where a ZCS arises at a corner of a system that is completely trivial both in bulk and in edge. If we assume $\lambda = 0$ and $|t| > |g|$ in $h^{(4)}$, the resulting band structure in Fig. 3(i) does not carry nonzero bulk polarization nor corner charge at any bands. This model does not support any edge-localized bands as well. Surprisingly, however, a ZCS is still present as shown in Fig. 3(j)-(k), clearly demonstrating that it is possible to obtain a corner defect state without any topological origin. In this sense, the present model $h^{(4)}(|t| > |g|; \lambda = 0)$ serves as a pedagogical example that any corner states should not be assumed topological unless there is a concrete causal relationship between them and a certain topological invariant.

In conclusion, we addressed that a topological correspondence between a corner state and a nontrivial bulk invariant should be claimed by a physical argument (e.g. a half charge with chiral symmetry), but not by coincidence of their existence conditions in terms of the Hamiltonian parameters. Our two primary examples clearly demonstrated that the bulk polarization in C^3 - and C^4 -symmetric crystalline insulators and the corresponding fractional corner charge anomaly is not correlated with the emergence of the corner states at zero energy. We lastly showed that a corner state can appear even in a completely trivial insulator, which further strengthens our point that a corner-localized state qualifies as an indicator of higher-order topology only when a solid bulk-corner correspondence precedes.

This work was supported by the Army Research Office (ARO) under a Grant No. W911NF-16-1-0319, and by the National Science Foundation (NSF) under the Grants No. DMR-1741788 and DMR-1719875. M.J. was also supported in part by Cornell Fellowship and in part by the Kwanjeong Fellowship from Kwanjeong Educational Foundation.

* mj397@cornell.edu

† gshvets@cornell.edu

- [1] A. P. Schnyder, S. Ryu, A. Furusaki, and A. W. W. Ludwig, *Phys. Rev. B* **78**, 195125 (2008).
- [2] S. Ryu, A. P. Schnyder, A. Furusaki, and A. W. W. Ludwig, *New J. Phys.* **12**, 065010 (2010).
- [3] L. Fidkowski, T. S. Jackson, and I. Klich, *Phys. Rev. Lett.* **107**, 036601 (2011).
- [4] G. M. Graf and M. Porta, *Commun. Math. Phys.* **324**, 851 (2013).
- [5] K. Shiozaki and M. Sato, *Phys. Rev. B* **90**, 165114 (2014).
- [6] M. Sitte, A. Rosch, E. Altman, and L. Fritz, *Phys. Rev. Lett.* **108**, 126807 (2012).
- [7] W. A. Benalcazar, B. A. Bernevig, and T. L. Hughes, *Science* **357**, 61 (2017).
- [8] Z. Song, Z. Fang, and C. Fang, *Phys. Lett. Rev.* **119**, 246402 (2017).
- [9] J. Langbehn, Y. Peng, L. Trifunovic, F. von Oppen, and P. W. Brouwer, *Phys. Lett. Rev.* **119**, 246401 (2017).
- [10] F. Schindler, A. M. Cook, M. G. Vergniory, Z. Wang, S. S. P. Parkin, B. A. Bernevig, and T. Neupert, *Sci. Adv.* **4**, eaat0346 (2018).
- [11] F. Schindler, Z. Wang, M. G. Vergniory, A. M. Cook, A. Murani, S. Sengupta, A. Y. Kasumov, R. Deblock, S. Jeon, I. Drozdov, H. Bouchiat, S. Guéron, A. Yazdani, B. A. Bernevig, and T. Neupert, *Nat. Phys.* **14**, 918 (2018).
- [12] J. Noh, W. A. Benalcazar, S. Huang, M. J. Collins, K. P. Chen, T. L. Hughes, and M. C. Rechtsman, *Nat. Photon.* **12**, 408 (2018).
- [13] C. W. Peterson, W. A. Benalcazar, T. L. Hughes, and G. Bahl, *Nature (London)* **555**, 346 (2018).
- [14] M. Serra-Garcia, V. Peri, R. Süssstrunk, O. R. Bilal, T. Larsen, L. G. Villanueva, and S. D. Huber, *Nature (London)* **555**, 342 (2018).
- [15] S. Mittal, V. V. Orre, G. Zhu, M. A. Gorlach, A. Poddubny, and M. Hafezi, *Nat. Photon.* **13**, 692 (2019).
- [16] M. Geier, L. Trifunovic, M. Hoskam, and P. W. Brouwer, *Phys. Rev. B* **97**, 205135 (2018).
- [17] L. Trifunovic and P. W. Brouwer, *Phys. Rev. X* **9**, 011012 (2019).
- [18] R. Takahashi, Y. Tanaka, , and S. Murakami, *Phys. Rev. Res.* **2**, 013300 (2020).
- [19] W. A. Benalcazar, T. Li, and T. L. Hughes, *Phys. Rev. B* **99**, 245151 (2019).
- [20] C. W. Peterson, T. Li, W. A. Benalcazar, T. L. Hughes, and G. Bahl, *Science* **368**, 1114 (2020).
- [21] X. Ni, M. Weiner, A. Alu, and A. B. Khanikaev, *Nat. Mater.* **18**, 113 (2019).
- [22] H. Xue, Y. Yang, F. Gao, Y. Chong, and B. Zhang, *Nat. Mater.* **18**, 108 (2019).
- [23] S. N. Kempkes, M. R. Slot, J. J. van den Broeke, P. Capiod, W. A. Benalcazar, D. Vanmaekelbergh, D. Bercioux, I. Swart, and C. M. Smith, *Nat. Mater.* **18**, 1292 (2019).
- [24] W. A. Benalcazar and A. Cerjan, *Phys. Rev. B* **101**, 161116(R) (2020).
- [25] D. J. Thouless, M. Kohmoto, M. P. Nightingale, and M. den Nijs, *Phys. Rev. Lett.* **49**, 405 (1982).
- [26] Y. Hatsugai, *Phys. Rev. Lett.* **71**, 3697 (1993).
- [27] G. van Miert and C. Ortix, *Phys. Rev. B* **96**, 235130 (2017).
- [28] W. A. Benalcazar, B. A. Bernevig, and T. L. Hughes, *Phys. Rev. B* **96**, 245115 (2017).
- [29] M. Xiao, G. Ma, Z. Yang, P. Sheng, Z. Q. Zhang, and C. T. Chan, *Nat. Phys.* **11**, 240 (2015).
- [30] Z. Fan, S. Dutta-Gupta, R. Gladstone, S. Trendafilov, M. Bosch, M. Jung, G. R. S. Iyer, A. J. Giles, M. Shcherbakov, B. Feigelson, J. D. Caldwell, M. Allen, J. Allen, and G. Shvets, *Nanophotonics* **8**, 1417 (2019).
- [31] M. Jung, R. Gladstone, and G. Shvets, *Adv. Photon.* **2**, 46003 (2020).
- [32] L. He, Z. Addison, E. J. Mele, and B. Zhen, *Nat. Commun.* **11**, 3119 (2020).